



Research Article

Surface Effects on the Scattering of SH-Wave Around an Arbitrary Shaped Nano-Cavity

Hongmei Wu ^{1,2} and Zhiying Ou ²

¹*School of Mechanical and Electrical Engineering, Lanzhou University of Technology, Lanzhou, Gansu, China*

²*School of Science, Lanzhou University of Technology, Lanzhou, Gansu, China*

Correspondence should be addressed to Zhiying Ou; zhiyingou@163.com

Received 2 July 2019; Revised 25 August 2019; Accepted 9 September 2019; Published 15 December 2019

Academic Editor: Antonio Scarfone

Copyright © 2019 Hongmei Wu and Zhiying Ou. This is an open access article distributed under the Creative Commons Attribution License, which permits unrestricted use, distribution, and reproduction in any medium, provided the original work is properly cited.

By using the complex variable function theory and the conformal mapping method, the scattering of plane shear wave (SH-wave) around an arbitrary shaped nano-cavity is studied. Surface effects at the nanoscale are explained based on the surface elasticity theory. According to the generalized Yong–Laplace equations, the boundary conditions are given, and the infinite algebraic equations for solving the unknown coefficients of the scattered wave solutions are established. The numerical solutions of the stress field can be obtained by using the orthogonality of trigonometric functions. Lastly, the numerical results of dynamic stress concentration factor around a circular hole, an elliptic hole and a square hole as the special cases are discussed. The numerical results show that the surface effect and wave number have a significant effect on the dynamic stress concentration, and prove that our results from theoretical derivation are correct.

1. Introduction

Since the scattering problem plays an important role in understanding the propagation phenomena of various waves in engineering materials and structures, the elastic wave scattering by the cavity embedded in the elastic matrix have always been a hot topic in wave motion theory. The application and development of mineral exploration, petroleum acquisition, quantitative nondestructive exploration, radar, underwater sonar, blasting and other technologies are all based on understanding the relationship between the scattering of elastic waves and the geometrical dimensions and physical parameters of defective bodies in elastic matrix. Pao and Mow [1] discussed in detail the diffraction of elastic waves in cavity/inclusion in an elastic medium by the methods of wave functions expansion, integral equation, and integral transform method. Using the complex variable function theory, Liu [2] discussed the dynamic stress concentration around a circular hole caused by SH-wave in an anisotropic medium. Subsequently, Liu et al. [3, 4] studied the scattering of SH-wave around an elliptical hole and cracks. In recent years, the scattering of circular cavity in circular domain to SH waves was analyzed by Wang and Jiang [5]. Liu et al. [6] discussed the

scattering of plane SH-waves by an arbitrary shaped cavity embedded in a wedge-shaped domain by the method of IBEM. Then Yang et al. [7, 8] studied the scattering of shear waves by a circular or an elliptical cavity in inhomogeneous medium. Further, Ghafarollahi and Shodja [9] proposed an analytical treatment for the scattering of SH-waves by an elliptical cavity/crack which is embedded near the interface between exponentially graded and homogeneous half-spaces.

However, the above studies were carried out at the macroscale, so the influence of the surface stresses was not considered. With the rapid development of nanotechnology, it is necessary to understand the mechanical behavior of nanomaterials and nanostructures. At the nano-scale, the surface effect becomes significant due to the increasing ratio of surface to bulk volume [10]. The surface elasticity theory that considers the surface/interface influences were proposed by Gurtin et al. [11], and Miller and Shenoy's [12, 13] results agreed with the surface elasticity theory. Subsequently, a geometric illustration to prove the generalized Yong–Laplace equation was presented by Chen et al. [14]. Therefore, the surface elasticity theory has been widely applied to study the various mechanical behaviors of materials and constructors at nano-scale [15–17].

By using the surface elasticity theory, Wang et al. [18, 19] considered the diffractions of P -wave by a nano-cavity. Further, Ou and Lee [20] discussed the effects of interface energy on the scattering of plane elastic wave by a nano-sized coated fiber. Ru et al. [21–23] studied the diffraction of the elastic waves around a cylindrical nano-inclusion and then studied the surface effects of the scatterings of the vertical shear wave by a cluster of nanosized cylindrical holes. Wu and Ou [24, 25] studied the interface effects of SH-waves' scattering around a cylindrical nano-inclusion by wave functions expansion method and complex variable function theory respectively. However, thanks to the complex boundary conditions of the arbitrary shaped cavity, most of those studies are confined to the circular hole or the spherical cavity/inclusion at the nano-size. Up to now, very few studies thought about the scattering of SH-wave by an arbitrary shaped nano-cavity. Therefore, it is necessary for us to study the relevant contents of the issue.

In this work, based on the theory of surface elasticity, the scattering of SH-wave around an arbitrary shaped nano-cavity embedded in an infinite elastic medium is studied, in which the numerical solutions of displacement fields are expressed by employing the complex variable function theory and the conformal mapping. The numerical results of dynamic stress concentration factor about a circular hole, an elliptic hole are illustrated graphically. The effects of surface energy on the dynamic stress concentration factor in the matrix material are analyzed. The paper is organized as follows. Section 2 briefly introduces the theory of surface elasticity. The solution for SH wave field around an arbitrary shaped nano-cavity is obtained using the method of conformal mapping. The governing equation and the corresponding boundary condition for the problem under consideration are presented in Section 3. In Section 4 discusses the surface effects on the dynamical stress concentration induced by incident SH-wave with a circular hole and an elliptic hole. The conclusions are presented in Section 5.

2. Surface Elasticity

According to the surface elasticity theory, a surface is considered to be a negligibly film that adheres to the matrix without slipping. The equilibrium equations and the isotropic constitutive relations in the matrix are the same as those in the classical theory of elasticity, but the presence of surface stress leads to nonclassical boundary conditions. To learn more about it, refer to Gurtin [11].

The surface stress tensor $\sigma_{\alpha\beta}^{(\text{sur})}$ and the surface energy density $G(\varepsilon_{\alpha\beta})$ satisfy the following formula

$$\sigma_{\alpha\beta}^{(\text{sur})} = G\delta_{\alpha\beta} + \frac{\partial G}{\partial \varepsilon_{\alpha\beta}}, \quad (1)$$

where $\varepsilon_{\alpha\beta}$ is the second-rank tensor of surface strain, $\delta_{\alpha\beta}$ is the Kronecker delta. All repeated Latin indices (1, 2, 3) and Greek indices (1, 2) in the entire paper use Einstein's summation convention.

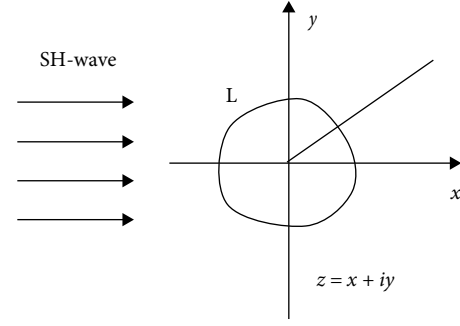


FIGURE 1: The scattering of SH-wave around an arbitrary shaped nano-cavity.

Based on the generalized Yong–Laplace equation [14], the equilibrium equations and the constitutive relations on the surface are

$$\sigma_{\alpha\beta}^{(\text{sur})} = \tau^0 \delta_{\alpha\beta} + 2(\mu^{(\text{sur})} - \tau^0) \delta_{\alpha\gamma} \varepsilon_{\gamma\beta} + (\lambda^{(\text{sur})} + \tau^0) \varepsilon_{\gamma\gamma} \delta_{\alpha\beta}. \quad (2)$$

$$(\sigma - \sigma^{(I)})\mathbf{n} = -\nabla_s \cdot \sigma^{(\text{sur})}, \quad (3)$$

where σ , $\sigma^{(I)}$, $\sigma^{(\text{sur})}$ are the stress tensors of the matrix, the inclusion, and the surface, respectively, \mathbf{n} denotes the normal vector of the surface, and $\nabla_s \cdot \sigma^{(\text{sur})}$ is the interface divergence. $\mu^{(\text{sur})}$ and $\lambda^{(\text{sur})}$ are two surface constants. The residual surface tension τ^0 is not considered in our dynamic analysis, i.e. $\tau^0 = 0$.

Since the classical elastic theory is established in the matrix, the equilibrium equations and isotropic constitutive relations are written as

$$\sigma_{ij,j} = \rho \frac{\partial^2 u_i}{\partial t^2}, \quad (4)$$

$$\sigma_{ij} = 2\mu \left(\varepsilon_{ij} + \frac{\nu}{1-\nu} \varepsilon_{kk} \delta_{ij} \right), \quad (5)$$

where t is the time, ρ is the mass density of the material, μ and ν are the shear modulus and the Poisson's ratio, respectively, and σ_{ij} , ε_{ij} are stress tensor and strain tensor in the matrix material, respectively. u_i is the component of displacement, and the strain tensor is related to the displacement vector \mathbf{u} by

$$\varepsilon_{ij} = \frac{1}{2} (u_{i,j} + u_{j,i}). \quad (6)$$

3. The Scattering of SH-Wave Around an Arbitrary Shaped Nano-Cavity

Based on surface elasticity theory, we discuss the scattering of SH-wave by an arbitrary shaped nano-cavity embedded in an infinite elastic medium, as shown in Figure 1.

The anti-plane governing equation in the matrix is

$$\frac{\partial \sigma_{xz}}{\partial x} + \frac{\partial \sigma_{yz}}{\partial y} = \rho \frac{\partial^2 w}{\partial t^2}, \quad (7)$$

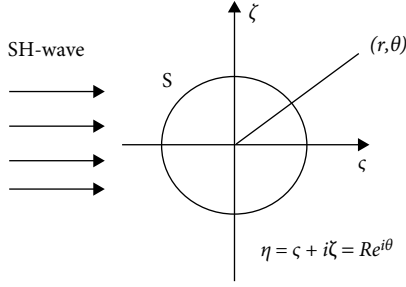


FIGURE 2: The conformal mapping of an arbitrary shaped nano-cavity.

where σ_{xz} , σ_{yz} are the shear stresses in the bulk. w is the displacement along the z axis.

The relations between stresses and displacement are

$$\sigma_{xz} = \mu \frac{\partial w}{\partial x}, \quad \sigma_{yz} = \mu \frac{\partial w}{\partial y}. \quad (8)$$

By substituting Equation (8) into Equation (7), we obtain

$$\frac{\partial^2 w}{\partial x^2} + \frac{\partial^2 w}{\partial y^2} = \frac{\rho}{\mu} \frac{\partial^2 w}{\partial t^2}. \quad (9)$$

For the steady-state response, the time can be separated as $w = W e^{-i\omega t}$, then Equation (9) can be expressed as

$$\nabla^2 W + K^2 W = 0, \quad (10)$$

where W is the displacement function, $K = \omega/v$ is the wave number, $v = \sqrt{\mu/\rho}$ is the shear velocity of the media, ω is the circular frequency, and ρ is the mass density.

Based on the complex variable function theory, we introduce complex variables $z = x + iy$, $\bar{z} = x - iy$. Equations (10) and (8) are

$$\frac{\partial^2 W}{\partial z \partial \bar{z}} + \frac{1}{4} K^2 W = 0. \quad (11)$$

$$\sigma_{xz} = \mu \left(\frac{\partial W}{\partial z} + \frac{\partial W}{\partial \bar{z}} \right), \quad \sigma_{yz} = i\mu \left(\frac{\partial W}{\partial z} - \frac{\partial W}{\partial \bar{z}} \right). \quad (12)$$

In order to solve the scattering of the noncircular cavity, the mapping function maps the arbitrary shaped nano-cavity boundary L of the z -plane to a conformal circle of radius R with the boundary S of the η -plane, as shown in Figure 2.

Introduce the conformal mapping function

$$z = g(\eta), \quad \eta = R e^{i\theta}. \quad (13)$$

Substituting the mapping function into Equation (11), the following equation is obtained

$$\frac{1}{g'(\eta)g'(\eta)} \frac{\partial^2 W}{\partial \eta \partial \bar{\eta}} + \frac{1}{4} K^2 W = 0, \quad (14)$$

Introducing the cylindrical coordinates (r, θ, z) , in η -plane, we have

$$\begin{aligned} \sigma_{rz} &= \frac{\mu}{R|g'(\eta)|} \left(\eta \frac{\partial W}{\partial \eta} + \bar{\eta} \frac{\partial W}{\partial \bar{\eta}} \right), \\ \sigma_{\theta z} &= \frac{i\mu}{R|g'(\eta)|} \left(\eta \frac{\partial W}{\partial \eta} - \bar{\eta} \frac{\partial W}{\partial \bar{\eta}} \right). \end{aligned} \quad (15)$$

Assume that a harmonically plane SH-wave propagates in the positive x -direction, as shown in Figure 2. According to Equation (11), the general solution of incident plane SH-wave function $W^{(\text{Inc})}$ in the cylindrical coordinates is expressed as [1]

$$W^{(\text{Inc})} = \frac{1}{2} W_0 \sum_{n=0}^{+\infty} \varepsilon_n i^n J_n [K|g(\eta)|] \left[\left(\frac{g(\eta)}{|g(\eta)|} \right)^n + \left(\frac{g(\eta)}{|g(\eta)|} \right)^{-n} \right], \quad (16)$$

where W_0 is the amplitude of the incident wave, $J_n(\cdot)$ is the n th order Bessel function of the first kind, and the coefficient $\varepsilon_n = 1$ for $n = 0$ and $\varepsilon_n = 2$ for $n \geq 1$.

The scattered wave function $W^{(\text{Sca})}$ in the cylindrical coordinates is expressed as [1]

$$W^{(\text{Sca})} = \frac{1}{2} W_0 \sum_{n=0}^{+\infty} a_n H_n^{(1)} [K|g(\eta)|] \left[\left(\frac{g(\eta)}{|g(\eta)|} \right)^n + \left(\frac{g(\eta)}{|g(\eta)|} \right)^{-n} \right], \quad (17)$$

where $H_n^{(1)}(\cdot)$ is the n th order Hankel function of the first kind, and a_n are unknown coefficients to be determined by the boundary conditions.

The total wave function in the matrix is given by the addition of $W^{(\text{Inc})}$ and $W^{(\text{Sca})}$

$$W = W^{(\text{Inc})} + W^{(\text{Sca})}. \quad (18)$$

According to the Equations (15)–(17), we can obtain

$$\sigma_{rz}^{(\text{Inc})} = \frac{K\mu W_0}{4R} \sum_{n=0}^{\infty} \varepsilon_n i^n (\varphi_1 + \varphi_2), \quad (19)$$

$$\sigma_{\theta z}^{(\text{Inc})} = \frac{iK\mu W_0}{4R} \sum_{n=0}^{\infty} \varepsilon_n i^n (\varphi_1 - \varphi_2), \quad (20)$$

$$\sigma_{rz}^{(\text{Sca})} = \frac{K\mu W_0}{4R} \sum_{n=0}^{\infty} a_n (\psi_1 + \psi_2), \quad (21)$$

$$\sigma_{\theta z}^{(\text{Sca})} = \frac{iK\mu W_0}{4R} \sum_{n=0}^{\infty} a_n (\psi_1 - \psi_2), \quad (22)$$

where

$$\begin{aligned} \varphi_1 &= \left[J_{n-1} [K|g(\eta)|] \left(\frac{g(\eta)}{|g(\eta)|} \right)^{n-1} - J_{n-1} [K|g(\eta)|] \left(\frac{g(\eta)}{|g(\eta)|} \right)^{-(n+1)} \right] \\ &\quad \cdot \frac{\eta g'(\eta)}{|g'(\eta)|}. \end{aligned} \quad (23)$$

$$\phi_2 = \left[\frac{J_{n-1}[K|g(\eta)|] \left(\frac{g(\eta)}{|g(\eta)|} \right)^{-n-1} - J_{n+1}[K|g(\eta)|] \left(\frac{g(\eta)}{|g(\eta)|} \right)^{(n+1)}}{\eta g'(\eta)} \right] \cdot \frac{\eta g'(\eta)}{|g'(\eta)|} \quad (24)$$

$$\psi_1 = \left[\frac{H_{n-1}^{(1)}[K|g(\eta)|] \left(\frac{g(\eta)}{|g(\eta)|} \right)^{n-1} - H_{n+1}^{(1)}[K|g(\eta)|] \left(\frac{g(\eta)}{|g(\eta)|} \right)^{-(n+1)}}{\eta g'(\eta)} \right] \cdot \frac{\eta g'(\eta)}{|g'(\eta)|} \quad (25)$$

$$\Psi_2 = \left[\frac{H_{n-1}^{(1)}[K|g(\eta)|] \left(\frac{g(\eta)}{|g(\eta)|} \right)^{-n-1} - H_{n+1}^{(1)}[K|g(\eta)|] \left(\frac{g(\eta)}{|g(\eta)|} \right)^{n+1}}{\eta g'(\eta)} \right] \cdot \frac{\eta g'(\eta)}{|g'(\eta)|} \quad (26)$$

The corresponding stresses are

$$\sigma_{rz} = \sigma_{rz}^{(\text{Inc})} + \sigma_{rz}^{(\text{Sca})}, \quad \sigma_{\theta z} = \sigma_{\theta z}^{(\text{Inc})} + \sigma_{\theta z}^{(\text{Sca})}. \quad (27)$$

According to the Equations (1)–(6), we can obtain the boundary condition on the surface ($r = R$)

$$\sigma_{rz} = -s \frac{\partial \sigma_{\theta z}}{\partial \theta}, \quad (28)$$

where $s = \mu^{(\text{sur})}/\mu R$, which is a dimensionless parameter that reflects the effect of surface at nano-scale. For a macroscopic cavity, the radius R is large enough ($s \ll 1$). Therefore, there is no need to consider surface effects. However, when the radius R of the hole is reduced to the nano-scale, s becomes apparent and the surface effect should be considered [26–28].

Substituting Equations (19)–(27) into Equation (28), we have

$$\sum_{n=0}^{+\infty} a_n (N^{(2)} - sN^{(1)}) = \sum_{n=0}^{+\infty} \varepsilon_n i^n (sM^{(1)} - M^{(2)}), \quad (29)$$

where $M^{(1)}$, $M^{(2)}$, $N^{(1)}$, $N^{(2)}$ are presented in Appendix.

It is evident that Equation (29) is an equation related to θ though there are still some unknown coefficients. Multiplying both sides of Equation (29) by $e^{-im\theta}$, then integrating respect to θ between the limits $-\pi$ and π , we obtain

$$\begin{aligned} \sum_{n=0}^{+\infty} a_n \int_{-\pi}^{\pi} (N^{(2)} - sN^{(1)}) e^{-im\theta} d\theta \\ = \sum_{n=0}^{+\infty} \varepsilon_n i^n \int_{-\pi}^{\pi} (sM^{(1)} - M^{(2)}) e^{-im\theta} d\theta. \end{aligned} \quad (30)$$

From Equation (30), an infinite algebraic equation about unknown constants a_n can be obtained. By solving the Equation (30), the unknown constants a_n can be calculated. It should be noted that it is mathematically convenient to truncate the infinite algebraic equation in Equation (30) with $n = m$ during numerical calculation.

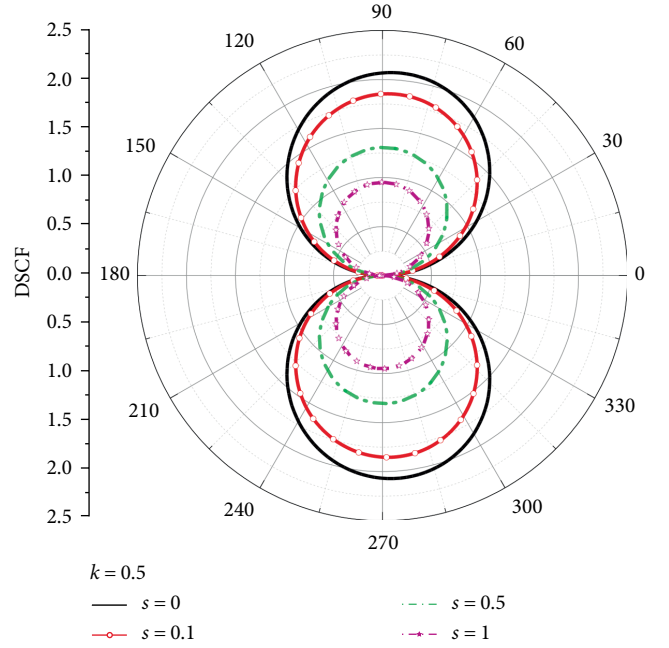


FIGURE 3: Distributions of DSCF around a circular hole with various s for $K = 0.5$.

4. Numerical Results and Discussion

In order to study the effect of surface effects on dynamic stress concentration factors (DSCF), we define DSCF to be

$$\text{DSCF} = \left| \frac{\sigma_{\theta z}}{\sigma_0} \right|, \quad (31)$$

where $\sigma_{\theta z}$ is the bulk stress in the medium along the surface, and $\sigma_0 = \mu K W_0$ is the stress intensity in the propagation direction of SH-wave. From the Equation (30), It is easy to see that surface elasticity parameter s has a great impact on DSCF.

In what follows, as special cases, we discuss the influence of the surface effects on the DSCF around a circular hole and an elliptic hole.

4.1. Circular Hole. For a circular hole, the expression of z can be written as

$$z = g(\eta) = \eta, \quad \eta = \zeta + i\zeta = R e^{i\theta}. \quad (32)$$

Substituting Equation (32) into Equation (30), the coefficients a_n can be determined as

$$a_n = -\varepsilon_n i^n \frac{(ns-1)J_{n-1}(KR) + (ns+1)J_{n+1}(KR)}{(ns-1)H_{n-1}^{(1)}(KR) + (ns+1)H_{n+1}^{(1)}(KR)}, \quad (33)$$

$(n = 0, 1, 2 \dots)$.

For a macroscopic circular hole, the surface effect is ignored ($s = 0$), our results for a_n are consistent with results of [1].

Thus, it is evident to see that our methods are correct, and the elastic stress fields the SH-wave induces can be obtained.

In order to consider the effects of surface on DSCF, the distributions of DSCF on the surface for different values of s with low frequency incident wave $K = 0.5$ are shown in Figure 3, which indicates obviously the surface effect on the

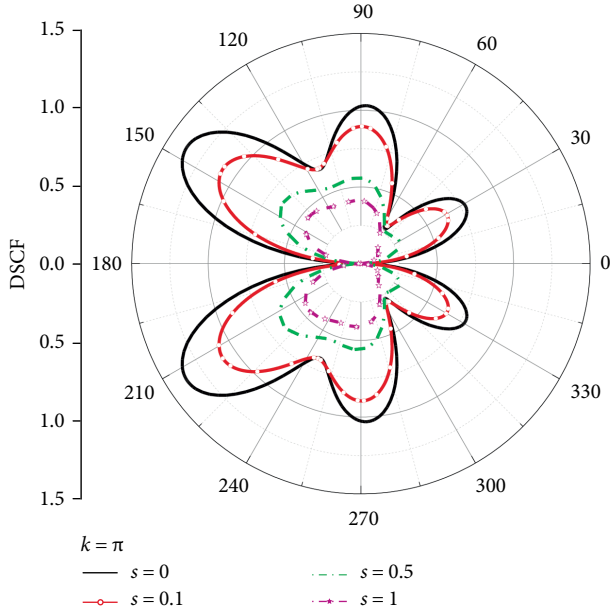


FIGURE 4: Distributions of DSCF around a circular hole with various s for $K = \pi$.

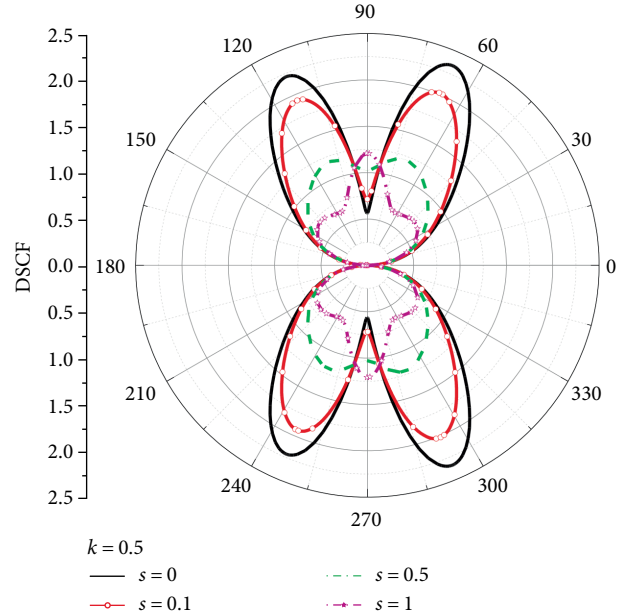


FIGURE 5: Distributions of DSCF around an elliptic hole with various s for $a = 1, b = 0.6, K = 0.5$.

DSCF near the hole. As s increases, the DSCF decreases continuously, the maximum DSCF decreases from 2.07 to 0.95. The maximum DSCF appears at about $\theta = \pm\pi/2$, and there are two peak values in the interval $(0, 2\pi)$. Similarly, the distributions of DSCF on the surface for different values of s with high frequency incident wave $K = \pi$ are shown in Figure 4, which also indicates obviously the surface effect on the DSCF near the hole. Again, as s increases, the DSCF decreases continuously too, the maximum DSCF decreases from 1.37 to 0.46. However, due to the high frequency, the distributions of DSCF changes frequently. The maximum value of DSCF occurs at angles of about $\theta = \pm 5\pi/6$.

4.2. *Elliptic Hole.* For an elliptic hole, the expression of z is written as

$$z = g(\eta) = c\left(\eta + \frac{d}{\eta}\right), \quad \eta = \zeta + i\zeta = Re^{i\theta}, \quad (34)$$

where $c = (a + b)/2, d = (a - b)/(a + b)$.

The distributions of DSCF on the surface for different values of s with $a = 1, b = 0.6$ and low frequency incident wave $K = 0.5$ are shown in Figure 5. It is remarkable that the surface effect on the DSCF near the elliptic hole. Compare with Figure 3, the results are similar to those for the circular hole in $(-23\pi/50, 23\pi/50)$ and $(27\pi/50, 73\pi/50)$, as s increases, the DSCF decreases continuously, while in $(23\pi/50, 27\pi/50)$ and $(73\pi/50, 77\pi/50)$, as s increases, the DSCF increases. However, the maximum DSCF appear at angles of about $\theta = \pm 7\pi/18$, and the maximum DSCF decreases from 2.34 to 1.21. Similarly, the distributions of DSCF on the surface for different values of s with high frequency incident wave $K = \pi$

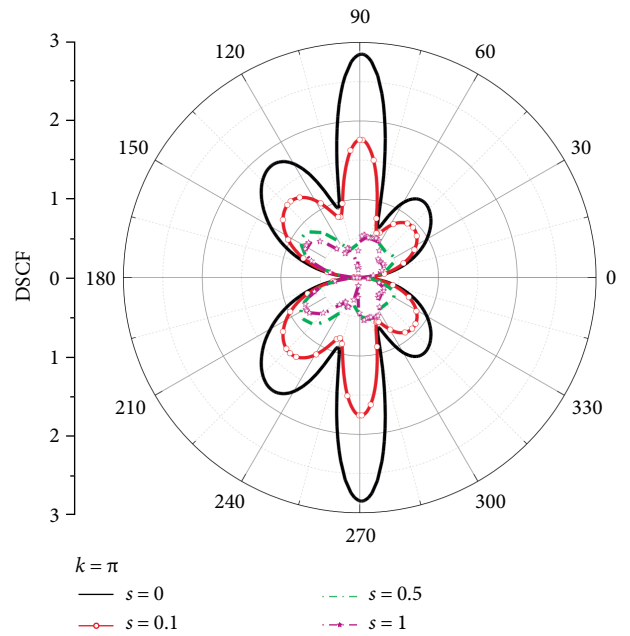


FIGURE 6: Distributions of DSCF around an elliptic hole with various s for $a = 1, b = 0.6, K = \pi$.

are shown in Figure 6, and the results are similar to those for $K = 0.5$ in most regions. However, for different s , the location of the maximum DSCF is different, the maximum DSCF decreases from 2.85 to 0.79. The change of DSCF at high frequency is larger than that at low frequency.

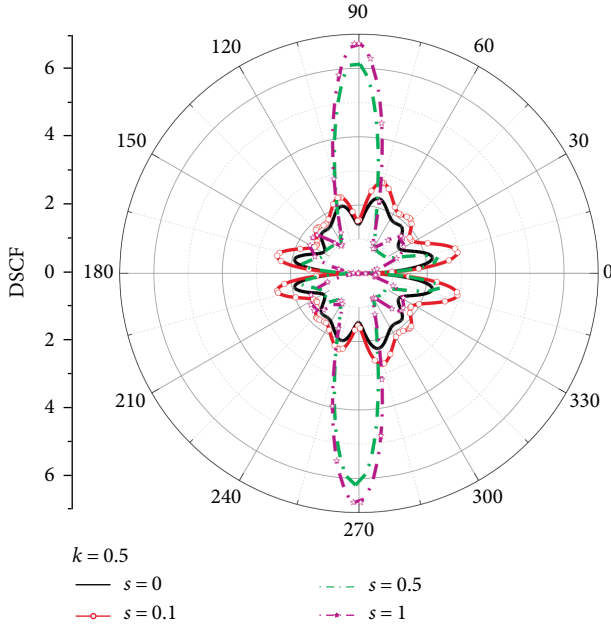


FIGURE 7: Distributions of DSCF around a square hole with various s for $K = 0.5$.

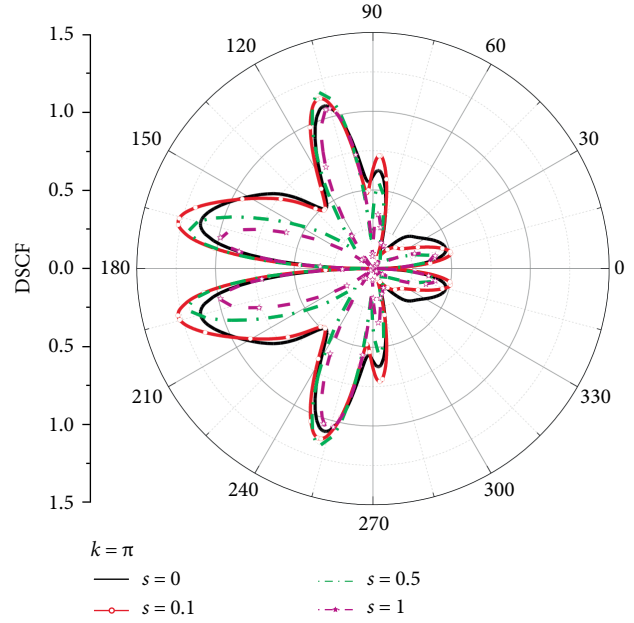


FIGURE 8: Distributions of DSCF around a square hole with various s for $K = \pi$.

4.3. *Square Hole.* For a square hole, the expression of z is written as

$$z = g(\eta) = \frac{1}{\eta} - \frac{1}{6}\eta^3, \quad \eta = \zeta + i\zeta = Re^{i\theta}. \quad (35)$$

The distributions of DSCF on the surface for different values of s with $K = 0.5$ are shown in Figure 7. It is remarkable that the surface effect on the DSCF near the square hole. Compare with Figures 3 and 5, the results are different from the circular hole and the elliptic hole, as s increases, the DSCF increases in $(5\pi/12, 7\pi/12)$ and $(17\pi/12, 19\pi/12)$, and in other intervals, the trend is not obvious. For different s , the location of the maximum DSCF is different. When $s = 0.5$ and $s = 1$, the changes are very significant. Similarly, the distributions of DSCF on the surface for different values of s with high frequency incident wave $K = \pi$ are shown in Figure 8, and the results are different from $K = 0.5$. For different s , the location of the maximum DSCF is approximately the same, the maximum DSCF appear at angles of about $\theta = 11\pi/12$ and $\theta = 13\pi/12$. However, due to the frequent disturbance of the incident wave and the complexity of the expression of $z = g(\eta)$, with the increases of s , there are no certain rule in the changes of DSCF.

It is evident from Figures 9 to 11 that the influence of the wave number is great on the DSCF. The DSCF decreases as K increases in most regions. Stress concentration around the square hole is more significant, the maximum value of DSCF is 6.19. However, the maximum value of DSCF is about 1.25 around the circular hole and the elliptical hole. In three cases, the symmetry of the DSCF with respect to $\theta = \pi$.

In summary, the numerical results show that the surface energy and the wave numbers have significant effects on the DSCF in the different shapes such as circular, ellipse or square.

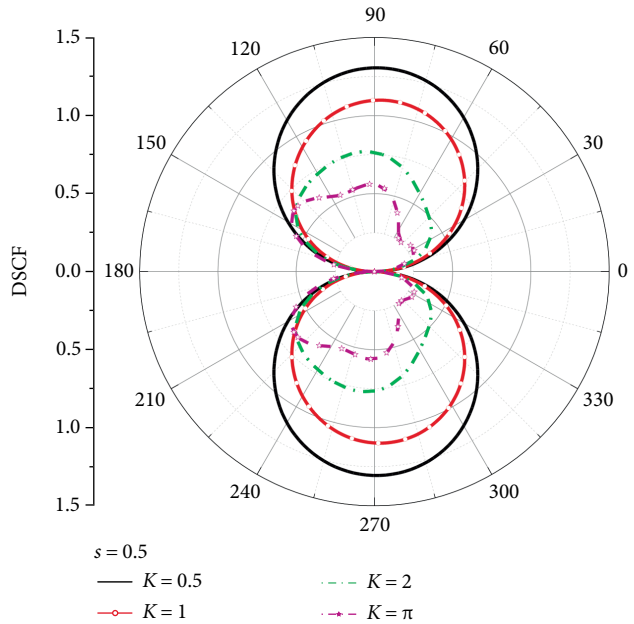


FIGURE 9: Distributions of DSCF around a circular hole with various K for $s = 0.5$.

5. Conclusion

In the present paper, we investigate the scattering of SH-wave by an arbitrary shaped nano-cavity embedded in an infinite elastic matrix based on the surface elasticity. By using the complex variable function theory and conformal mapping method, the numerical solutions of the stress field are obtained around the cavity. Simultaneously, the analytical solutions of the stress field around a circular hole are obtained. Finally, the obtained numerical results are used to analyze the influence of the

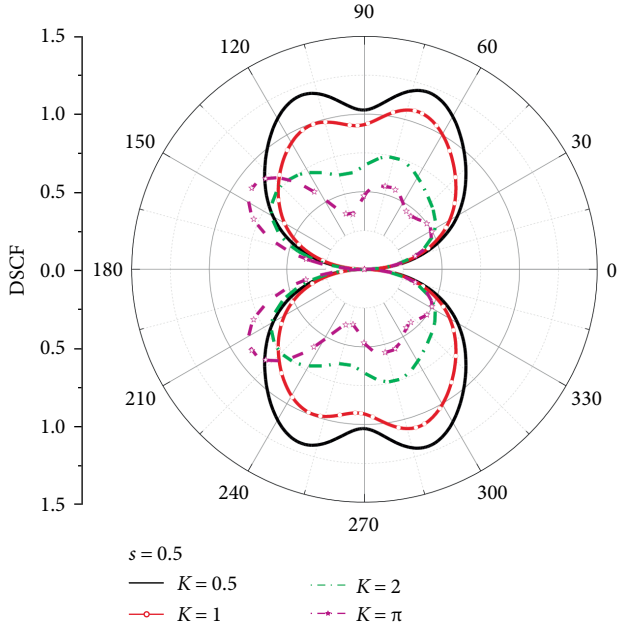


FIGURE 10: Distributions of DSCF around an ellipse hole with various K for $s = 0.5$.

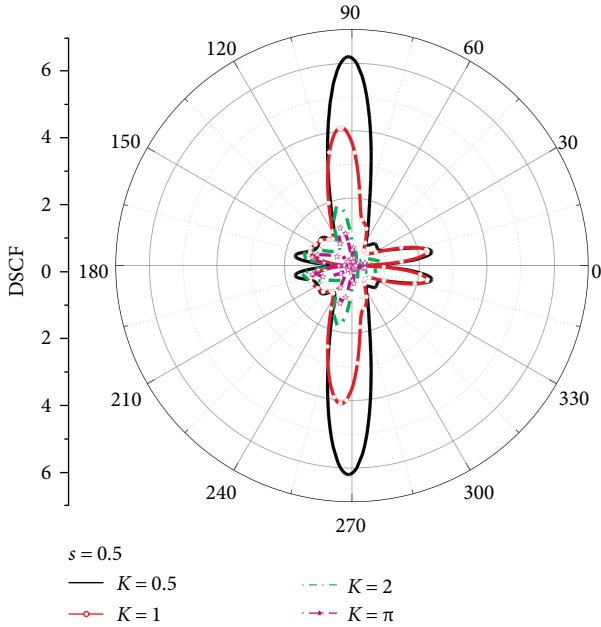


FIGURE 11: Distributions of DSCF around a square hole with various K for $s = 0.5$.

surface energy and the wave numbers on the DSCF around a circular hole, an ellipse hole and a square hole. When the radius of hole shrinks to nanometers, the surface effects become significant and should be taken into account. Regardless of the frequency of incident wave, the surface effect weakens the DSCF around the circular and ellipse hole in most regions, but it is different for the square hole. At the same time, the DSCF depends strongly on the wave numbers, with the wave numbers increases, the DSCF gradually decreases in most regions. This

study is helpful to analyze the mechanical properties of nonuniform nano-composites, such as the vibration of defective body models in micro-nano mechanical systems, the propagation of semiconductor nano-devices, and so on.

Appendix

Appendix A

$$M^{(1)} = \frac{K}{2} [(M_{11} + M_{12})P_1 + 2(M_{13} + M_{14})P_2 + (M_{15} + M_{16})\bar{P}_1] + \frac{1}{2} [(M_{21} - M_{22})P_3 + (M_{23} - M_{24})\bar{P}_3]. \quad (36)$$

$$M^{(2)} = (M_{21} - M_{22})P_4 + (M_{23} - M_{24})\bar{P}_4. \quad (37)$$

$$M_{11} = J_{n-2}[K|g(\eta)|] \left(\frac{g(\eta)}{|g(\eta)|} \right)^{n-2} \quad (38)$$

$$M_{12} = J_{n+2}[K|g(\eta)|] \left(\frac{g(\eta)}{|g(\eta)|} \right)^{-(n+2)}.$$

$$M_{13} = J_n[K|g(\eta)|] \left(\frac{g(\eta)}{|g(\eta)|} \right)^n \quad (39)$$

$$M_{14} = J_n[K|g(\eta)|] \left(\frac{g(\eta)}{|g(\eta)|} \right)^{-n}.$$

$$M_{15} = J_{n-2}[K|g(\eta)|] \left(\frac{g(\eta)}{|g(\eta)|} \right)^{-(n-2)} \quad (40)$$

$$M_{16} = J_{n+2}[K|g(\eta)|] \left(\frac{g(\eta)}{|g(\eta)|} \right)^{n+2}.$$

$$M_{21} = J_{n-1}[K|g(\eta)|] \left(\frac{g(\eta)}{|g(\eta)|} \right)^{n-1} \quad (41)$$

$$M_{22} = J_{n+1}[K|g(\eta)|] \left(\frac{g(\eta)}{|g(\eta)|} \right)^{-(n+1)}.$$

$$M_{23} = J_{n-1}[K|g(\eta)|] \left(\frac{g(\eta)}{|g(\eta)|} \right)^{-(n-1)} \quad (42)$$

$$M_{24} = J_{n+1}[K|g(\eta)|] \left(\frac{g(\eta)}{|g(\eta)|} \right)^{n+1}.$$

$$N^{(1)} = \frac{K}{2} [(N_{11} + N_{12})P_1 + 2(N_{13} + N_{14})P_2 + (N_{15} + N_{16})\bar{P}_1] + \frac{1}{2} [(N_{21} - N_{22})P_3 + (N_{23} - N_{24})\bar{P}_3]. \quad (43)$$

$$N^{(2)} = (N_{21} - N_{22})P_4 + (N_{23} - N_{24})\bar{P}_4. \quad (44)$$

$$N_{11} = H_{n-2}^{(1)}[K|g(\eta)|] \left(\frac{g(\eta)}{|g(\eta)|} \right)^{n-2} \quad (45)$$

$$N_{12} = H_{n+2}^{(1)}[K|g(\eta)|] \left(\frac{g(\eta)}{|g(\eta)|} \right)^{-(n+2)}.$$

$$N_{13} = H_n^{(1)}[K|g(\eta)|] \left(\frac{g(\eta)}{|g(\eta)|} \right)^n \quad (46)$$

$$N_{14} = H_n^{(1)}[K|g(\eta)|] \left(\frac{g(\eta)}{|g(\eta)|} \right)^{-n}.$$

$$N_{15} = H_{n-2}^{(1)}[K|g(\eta)|] \left(\frac{g(\eta)}{|g(\eta)|} \right)^{-(n-2)} \quad (47)$$

$$N_{16} = H_{n+2}^{(1)}[K|g(\eta)|] \left(\frac{g(\eta)}{|g(\eta)|} \right)^{n+2}.$$

$$N_{21} = H_{n-1}^{(1)}[K|g(\eta)|] \left(\frac{g(\eta)}{|g(\eta)|} \right)^{n-1} \quad (48)$$

$$N_{22} = H_{n+1}^{(1)}[K|g(\eta)|] \left(\frac{g(\eta)}{|g(\eta)|} \right)^{-(n+1)}.$$

$$N_{23} = H_{n-1}^{(1)}[K|g(\eta)|] \left(\frac{g(\eta)}{|g(\eta)|} \right)^{-(n-1)} \quad (49)$$

$$N_{24} = H_{n+1}^{(1)}[K|g(\eta)|] \left(\frac{g(\eta)}{|g(\eta)|} \right)^{n+1}.$$

$$P_1 = \frac{\eta^2 [g'(\eta)]^2}{|g'(\eta)|}, \bar{P}_1 = \frac{\bar{\eta}^2 \overline{[g'(\eta)]^2}}{|g'(\eta)|} \quad (50)$$

$$P_3 = \frac{2\eta g'(\eta) + \eta^2 g''(\eta)}{|g'(\eta)|} + \frac{|\eta|^2 [g'(\eta)]^2 \overline{g''(\eta)}}{|g'(\eta)|^3}$$

$$P_2 = |\eta^2| |g'(\eta)|, P_4 = \frac{\eta g'(\eta)}{|g'(\eta)|}, \bar{P}_4 = \frac{\bar{\eta} \overline{g'(\eta)}}{|g'(\eta)|} \quad (51)$$

$$\bar{P}_3 = \frac{2\bar{\eta} \overline{g'(\eta)} + \bar{\eta}^2 \overline{g''(\eta)}}{|g'(\eta)|} + \frac{|\eta|^2 \overline{[g'(\eta)]^2} g''(\eta)}{|g'(\eta)|^3}.$$

Data Availability

The data used to support the findings of this study are included within Figures 3–11 of the article.

Conflicts of Interest

The authors declare that they have no conflicts of interest.

Acknowledgment

This work was supported by the National Natural Science Foundation of China (Grant No. 11362009 and No. 11862014).

References

- [1] Y. H. Pao and C. C. Mow, *Diffraction of Elastic Waves and Dynamic Stress Concentrations*, Crane Russak, New York, NY, USA, 1973.
- [2] D. K. Liu, “Dynamic stress concentration around a circular hole due to SH-wave in anisotropic media,” *Acta Mechanica Sinica*, vol. 4, no. 2, pp. 146–155, 1988.
- [3] D. K. Liu and Z. G. Chen, “Scattering of SH-wave by cracks originating at an elliptic hole and dynamic stress intensity factor,” *Applied Mathematics and Mechanics*, vol. 25, no. 9, pp. 1047–1056, 2004.
- [4] Z. G. Chen, D. K. Liu, and Z. L. Yang, “Dynamic stress concentration and scattering of SH-wave by interface elliptic cylindrical cavity,” *Earthquake Engineering and Engineering Vibration*, vol. 2, no. 2, pp. 299–306, 2003.
- [5] P. Wang and S. T. Jiang, “Scattering of circular cavity in circular domain to SH waves,” *Journal of Mechanical Strength*, vol. 37, no. 1, pp. 18–22, 2015.
- [6] Z. Liu, L. Liu, and J. Liang, “Solving the scattering of plane SH-waves by an arbitrary shaped cavity embedded in a wedge-shaped space by IBEM,” *Acta Mechanica Solida Sinica*, vol. 35, no. 3, pp. 292–301, 2014.
- [7] Z. L. Yang, B. P. Hei, and Y. Wang, “Scattering by circular cavity in radially inhomogeneous medium with wave velocity variation,” *Applied Mathematics and Mechanics*, vol. 36, no. 5, pp. 599–608, 2015.
- [8] B. P. Hei, Z. L. Yang, and Z. G. Chen, “Scattering of shear waves by an elliptical cavity in a radially inhomogeneous isotropic medium,” *Earthquake Engineering and Engineering Vibration*, vol. 15, no. 1, pp. 145–151, 2016.
- [9] A. Ghafarollahi and H. M. Shodja, “Scattering of SH-waves by an elliptic cavity/crack beneath the interface between functionally graded and homogeneous half-spaces via multipole expansion method,” *Journal of Sound and Vibration*, vol. 435, pp. 372–389, 2018.
- [10] E. W. Wong, P. E. Sheehan, and C. M. Lieber, “Nanobeam mechanics: elasticity, strength and toughness of nanorods and nanotubes,” *Science*, vol. 277, no. 5334, pp. 1971–1975, 1997.
- [11] M. E. Gurtin, J. Weissmüller, and F. Larché, “A general theory of curved deformable interfaces in solids at equilibrium,” *Philosophical Magazine A*, vol. 78, no. 5, pp. 1093–1109, 1998.
- [12] R. E. Miller and V. B. Shenoy, “Size-dependent elastic properties of nanosized structural elements,” *Nanotechnology*, vol. 11, no. 3, pp. 139–147, 2000.
- [13] V. B. Shenoy, “Size-dependent rigidities of nanosized torsional elements,” *International Journal of Solids and Structures*, vol. 39, no. 15, pp. 4039–4052, 2002.
- [14] T. Chen, M. S. Chiu, and C. N. Weng, “Derivation of the generalized Young–Laplace equation of curved interfaces in

- nanoscaled solids,” *Journal of Applied Physics*, vol. 100, no. 7, p. 074308, 2006.
- [15] P. Sharma, S. Ganti, and N. Bhate, “Effect of surfaces on the size-dependent elastic state of nano-inhomogeneities,” *Applied Physics Letters*, vol. 82, no. 4, pp. 535–537, 2003.
- [16] Z. Y. Ou, G. F. Wang, and T. J. Wang, “Effect of residual surface tension on the stress concentration around a nanosized spheroidal cavity,” *International Journal of Engineering Science*, vol. 46, no. 5, pp. 475–485, 2008.
- [17] Z. Y. Ou, G. F. Wang, and T. J. Wang, “Elastic fields around a nanosized spheroidal cavity under arbitrary uniform remote loadings,” *European Journal of Mechanics A-Solids*, vol. 28, no. 1, pp. 110–120, 2009.
- [18] G. F. Wang, T. J. Wang, and X. Q. Feng, “Surface effects on the diffraction of plane compressional waves by a nanosized circular hole,” *Applied Physics Letters*, vol. 89, no. 23, p. 231923, 2006.
- [19] G. F. Wang, “Diffraction of plane compressional wave by a nanosized spherical cavity with surface effects,” *Applied Physics Letters*, vol. 90, no. 21, p. 211907, 2007.
- [20] Z. Y. Ou and D. W. Lee, “Effects of interface energy on scattering of plane elastic wave by a nano-sized coated fiber,” *Journal of Sound and Vibration*, vol. 331, no. 25, pp. 5623–5643, 2012.
- [21] Y. Ru, G. F. Wang, and T. J. Wang, “Diffraction of elastic waves and stress concentration near a cylindrical nano-inclusion incorporating surface effect,” *Journal of Vibration and Acoustics*, vol. 131, no. 6, pp. 1747–1750, 2009.
- [22] Y. Ru, G. F. Wang, L. C. Su, and T. J. Wang, “Scattering of vertical shear wave by a cluster of nanosized cylindrical holes with surface effect,” *Acta Mechanica*, vol. 224, no. 5, pp. 935–944, 2013.
- [23] Y. Ru, “Surface effect on diffractions of elastic waves and stress concentration near a cluster of cylindrical nanoholes arranged as quadrate shape,” *Advances in Materials Science and Engineering*, vol. 2015, Article ID 134975, 8 pages, 2015.
- [24] H. M. Wu and Z. Y. Ou, “Scattering of SH-wave by a cylindrical of nano-inclusion with interface effect,” in *Proceedings of the 2014 International Conference on Energy, Environment and Materials Engineering*, pp. 918–922, Guangdong, China 2014.
- [25] H. M. Wu, “Application of the complex variable function method to SH-wave scattering around a circular nano-inclusion,” *Advances in Mathematical Physics*, vol. 2019, Article ID 7203408, 8 pages, 2019.
- [26] P. Sharma and L. T. Wheeler, “Size-dependent elastic state of ellipsoidal nano-inclusions incorporating surface/interface tension,” *Journal of Applied Mechanics*, vol. 74, no. 3, pp. 447–454, 2007.
- [27] L. H. He and Z. R. Li, “Impact of surface stress on stress concentration,” *International Journal of Solids and Structures*, vol. 43, no. 20, pp. 6208–6219, 2006.
- [28] L. Tian and R. K. N. D. Rajapakse, “Elastic field of an isotropic matrix with a nanoscale elliptical inhomogeneity,” *International Journal of Solids and Structures*, vol. 44, no. 24, pp. 7988–8005, 2007.

